RESEARCH ARTICLE

Uniformly Distributed Palladium Nanoparticles on NH_2-MIL-53 Fabricated by an Equilibrium Adsorption Method for Reduction of Nitrite in Water

Yuan Huang,[a] Wontae Kim,[a] Ryoichi Otomo,[b] Shuhei Shimoda,[c] Kevin C.-W. Wu[d] and Yuichi Kamiya*[b]

[a] Yuan Huang and Dr. Wontae Kim
Graduate School of Environmental Science
Hokkaido University
Sapporo, 060-0810 Hokkaido (Japan)

[b] Prof. Dr. Ryoichi Otomo and Prof. Dr. Yuichi Kamiya
Faculty of Environmental Earth Science
Hokkaido University
Sapporo, 060-0810 Hokkaido (Japan)
E-mail: kamiya@ees.hokudai.ac.jp

[c] Shuhei Shimoda
Institute for Catalysis
Hokkaido University
Sapporo, 001-0021 Hokkaido (Japan)

[d] Prof. Dr. Kevin C.-W. Wu
Department of Chemical Engineering
National Taiwan University
Taipei, 10617 Taiwan (R. O. C.)

Supporting information for this article is given via a link at the end of the document.

Abstract: Metal particle on a support material should be small and homogeneous in size, which is desirable when using it as a catalyst. In this study, we investigated to introduce Pd nanoparticles (NPs) with narrow size distribution into NH_2-MIL-53, which was prepared by the reaction of aluminum(III) nitrate with 2-aminoterephthalic acid. Only by immersing it in an aqueous $PdCl_2$ solution, followed by the reduction with $NaBH_4$, Pd NPs of about 2 nm with unform distribution were formed in NH_2-MIL-53 up to 3.5 wt.% Pd loadings. Amino group on the linkers in NH_2-MIL-53 played a critical role for the introduction of $(PdCl_3)^-$ as a precursor for Pd NPs, while no Pd was introduced into MIL-53 without amino group. The obtained catalysts (Pd@NH_2-MIL-53) showed high catalytic performance for reduction of nitrite in water. The specific activity per Pd site exposed on the surface changed greatly depending on the Pd loadings despite the size of Pd NPs unchanged. Pd@NH_2-MIL-53 with low Pd loadings showed higher specific activity (TOF = 2.9×10^2 h^{-1}), which might be due to the preferential exposure of Pd(111) facet on Pd NPs.

Introduction

Metal-organic frameworks (MOFs) are a class of porous materials and constructed by the bonding between inorganic metal nodes and organic linkers to form periodic and high-dimensional crystalline networks.[1,2] By this, MOFs have special character of well-defined pore structure and high surface areas, which result in accelerated diffusion of reactant molecules into the pores. Thus, MOFs have attracted great attention to the application in heterogeneous catalysts. The coordinatively unsaturated metal sites in inorganic metal nodes can help adsorption and activation of reactant molecules, and some specific functional organic groups (e. g. amide, pyridyl) on organic linkers can also be active sites, getting MOFs to act as a catalyst.[3-6].

Besides the direct use of MOFs, use of MOFs as a support material for embedding and fixing catalytically active metal nanoparticles (MNPs) is a promising way to develop high performance catalysts. The three-dimensionally ordered structure and high porosity can facilitate uniform dispersion of MNPs, meanwhile can suppress the migration and aggregation of MNPs to avoid catalyst deactivation.[7-11] Furthermore, the functional groups on organic linkers in MOF can facilitate in controlling the electronic state of the dispersed metal species by charge transfer from the functional groups to metal species and *vice versa*.[12,13]

In the last decade, several approaches to prepare MNPs in MOFs (MNPs@MOF) have been reported, which include solvent-free gas-phase loading, incipient wetness impregnation, solid grinding and one-pot strategy, and the synthesized MNPs@MOF were applied as a catalyst for various organic conversion reactions, where the effects of functional groups in MOF and/or the pore structure were discussed.[14-17] For instance, two functional groups, which are $-SO_3H$ and $-NH_3^+$, were attached to UiO-66 to form UiO-66-S and UiO-66-N, respectively, and Pt nanoparticles (NPs) were further embedded into them.[18] It was found that those functional groups played a critical role in

selective conversion of methylcyclopentane, where Pt@UiO-66-S promoted the formation of C_6-cyclic products, while Pt@UiO-66-N facilitated that of acyclic isomer.[18]

Apart from the use in organic media, the application of MOF-catalysts in aqueous one is noteworthy from the viewpoint of environmentally benign organic synthesis, because water is considered as a non-toxic and environmentally benign solvent. Moreover, such use of MOF-catalysts is essential as water treatment, which is a huge task currently. However, a general concern is raised that MOFs do not have sufficient stability in water. In fact, most MOFs are highly sensitive to water, while high-valence metal ions like Al^{3+}, Fe^{3+}, Cr^{3+} and Zr^{4+} have been reported to give water stable MOFs, such as well-known UiO-66, PCN, MIL-53 and MIL-101.[19,20]

In this study, Al-based NH_2-MIL-53, which is an analogue of MIL-53, was chosen as a catalyst support to discuss the effect of amino group in the linker on the introduction of Pd NPs to the MOF and on catalytic performance in water. MIL-53 was first reported by Férey et al. in 2004, and is an aluminium dicarboxylate Al(OH)(BDC) (BDC=1,4-benzenedicarboxylate) which is isostructural to Cr-based MIL-53. The framework of Al-based MIL-53 is built up of infinite chains of corner-sharing $AlO_4(OH)_2$ octahedra interconnected with dicarboxylate groups in BDC, resulting in a crystalline structure containing one-dimensional diamond-shape channels with pores of free diameter close to 0.85 nm.[21] By using NH_2-BDC instead of BDC, NH_2-MIL-53 is synthesized under mild conditions.

Here, we wish to propose an easy way to introduce Pd NPs into NH_2-MIL-53, which is just immersing NH_2-MIL-53 in an aqueous solution of $PdCl_2$ (called equilibrium adsorption method here), followed by the reduction with $NaBH_4$. The obtained Pd@NH_2-MIL-53 was applied as a catalyst for reduction of nitrite (NO_2^-) with H_2 in water. A monometallic Pd system was selected in this study as it was easy to discuss the support effect on the catalytic performance rather than a bimetallic system. Nitrate (NO_3^-) is a pollutant commonly found in natural water and reduction of NO_3^- over bimetallic Pd catalysts like Pd-Cu, Pd-Sn and Pd-In gives NO_2^- as an intermediate product.[22-27] Since the reduction of NO_2^- proceeds over the Pd sites in the bimetallic Pd catalysts,[28-30] this reaction determines the selectivity between N_2 and NH_3 as the end products in the NO_3^- reduction (**Scheme 1**). Thus, studying the NO_2^- reduction has importance in demonstrating the usefulness of Pd@NH_2-MIL-53 as an environmental catalyst for water treatment.

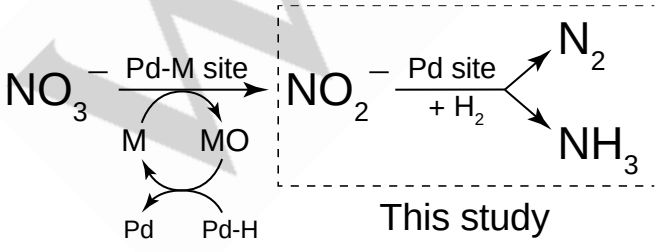

Scheme 1. Reaction pathway for NO_3^- reduction over a bimetallic Pd catalyst and the subject of this study.

Results and Discussion

Catalyst characterization

First, we investigated the influence of amino group in the organic linker on the introduction of Pd NPs by the equilibrium adsorption method. The amounts of Pd introduced in the samples, namely actual Pd loading, were determined by ICP-AES, and the results are listed in **Table 1**. For Pd@MIL-53 which does not have amino group on the organic linker, no Pd was introduced by the equilibrium adsorption method. In contrast, Pd was successfully introduced to NH_2-MIL-53 by this method as demonstrated in **Table 1**. For example, 2.1 wt.% Pd was loaded onto NH_2-MIL-53 when Pd equivalent to 3.0 wt.% was added (Pd@NH_2-MIL-53_2.1). A reasonable explanation why MIL-53 failed while NH_2-MIL-53 succeeded to take in Pd by the equilibrium adsorption method is that amino group in the organic linker acted as binding site for Pd species formed in an aqueous solution of $PdCl_2$. To know how the Pd species was introduced to NH_2-MIL-53, relationship between actual Pd loading and the amount of amino group was investigated.

Table 1. Added and actual Pd loadings, and specific surface areas for the samples

Sample	Method[a]	Pd loading (wt.%)		SA
		Added	Actual[b]	$m^2\ g^{-1}$
Pd@MIL-53	EA	3.0	~0[c]	---
Pd@NH_2-MIL-53_0.5	EA	0.5	0.5	289
Pd@NH_2-MIL-53_0.8	EA	1.0	0.8	154
Pd@NH_2-MIL-53_2.1	EA	3.0	2.1	161
Pd@NH_2-MIL-53_2.6	EA	5.0	2.6	263
Pd@NH_2-MIL-53_3.5	EA	8.0	3.5	205
Pd/NH_2-MIL-53	CI	3.0	3.2	56
Pd/MIL-53	CI	3.0	5.0	164
NH_2-MIL-53	---	---	---	401
MIL-53	---	---	---	1042

[a] EA: equilibrium adsorption method and CI: conventional impregnation method. [b] Determined by ICP-AES. [c] Not detected.

The amount of nitrogen was determined by chemical elemental analysis, and it was regarded as that of amino group present in NH_2-MIL-53. The result indicated that the amount of amino group was 3.18 mmol g^{-1}. **Figure 1(A)** shows the relationship between expected and actual Pd/N molar ratios for Pd@NH_2-MIL-53 with different Pd loadings, where the expected ratios were calculated from the amount of added Pd. As **Figure 1(A)** shows, the actual Pd/N molar ratio was increased with increase in the expected one but was always smaller than the latter even in the low Pd/N ratio. This implied that the interaction between amino group on the organic linker and the Pd species in the solution was not so strong that only a part of amino groups was occupied by the Pd species under the conditions in the equilibrium adsorption method. Hereafter, the actual Pd loading is called just Pd loading.

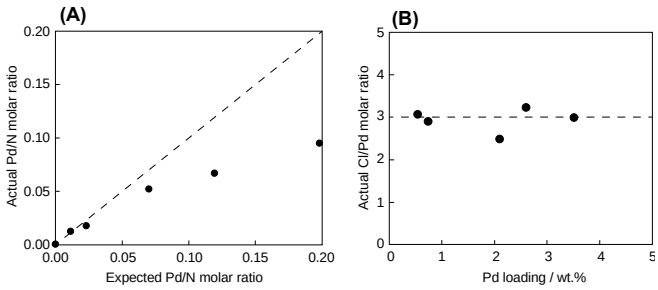

Figure 1. (A) Relationship between actual and expected Pd/N molar ratios and (B) relationship between Pd loading and actual Cl/Pd ratio for Pd@NH_2-MIL-53.

To know what Pd species was introduced to NH_2-MIL-53, the amounts of Cl in the samples after the introduction of Pd but before the reduction with $NaBH_4$ were determined. In **Figure 1(B)**, actual Cl/Pd ratios are plotted as a function of the Pd loadings. As **Figure 1(B)** demonstrates, the Cl/Pd molar ratios were always approximately 3 regardless of the Pd loadings. In a separate experiment, NH_2-MIL-53 was treated in dilute hydrochloric acid without $PdCl_2$, whose pH was adjusted to the same value as that in the $PdCl_2$ solution (pH 4), and it was found that no Cl was taken in NH_2-MIL-53. Therefore, it was obvious that Cl present in Pd@NH_2-MIL-53 before the $NaBH_4$ reduction were involved in the Pd species, meaning that three Cl were coordinated to one Pd atom. It is known that Pd species exists in an aqueous solution containing Cl^- as anionic chloropalladium(II) complexes including $(PdCl_4)^{2-}$, $(PdCl_3)^-$ and $[PdCl_3(H_2O)]^-$, or cationic ones like $(PdCl)^+$ and hydrated Pd^{2+}, or neutral $PdCl_2$, whose abundance ratio are changed depending on the concentrations of Pd^{2+} and Cl^-, and pH.[31] The fact that the actual Cl/Pd ratio was 3 indicated that $(PdCl_3)^-$ was a predominant species present in Pd@NH_2-MIL-53 before the $NaBH_4$ reduction. Since the aqueous $PdCl_2$ solution used in this study was acidic (pH 4), almost all amino groups in NH_2-MIL-53 must be protonated considering p*K*a of common amino groups. Therefore, $(PdCl_3)^-$ was electrostatically interacted with the protonated amino group forming an ion pair of $-NH_3^+$---$(PdCl_3)^-$. After the reduction with $NaBH_4$, Cl were completely removed from the samples, indicating that amino group was fully recovered without the Pd species in the resulting Pd@NH_2-MIL-53.

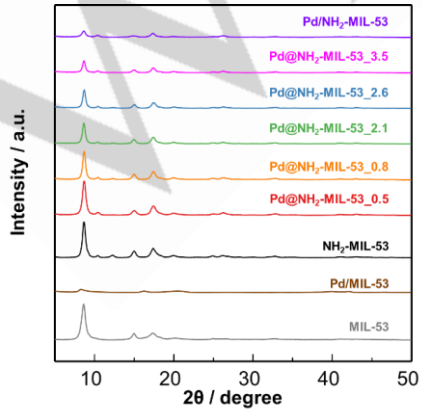

Figure 2. PXRD patterns of pristine MOFs and Pd-introduced ones.

The crystalline structures of pristine MOFs (MIL-53 and NH_2-MIL-53) and those after the introduction of Pd were investigated by PXRD. The PXRD pattern (**Figure 2**) of MIL-53 was basically identical to that in a previous paper[32] and NH_2-MIL-53 gave a PXRD pattern almost identical to that of MIL-53, indicating that amino group on the organic linker had little impact on the framework structure of the MOF. For Pd/NH_2-MIL-53 and Pd/MIL-53, which were prepared by a conventional impregnation method using the same $PdCl_2$ solution as that for Pd@NH_2-MIL-53, the intensities of the diffraction line at 2θ = 8.7°, which was assigned to (101) plane of the MOFs, were very weak comparing with those for the pristine MOFs, indicating that the framework structure was degraded. The $PdCl_2$ solution used in this study was prepared by dissolving $PdCl_2$ in hydrochloric acid, and then NaOH solution was added in order to adjust pH to 4. In the conventional impregnation method, this solution was gradually concentrated as the solvent (water) was evaporated, and eventually acidity of the solution became so high. MIL-53 and NH_2-MIL-53 are unstable in highly acidic solution[33] because the organic linker must exist as a carboxylate anion. Therefore, the framework structure of the MOFs collapsed during the introduction of the Pd species by the conventional impregnation method.

In contrast, Pd@NH_2-MIL-53 prepared by the equilibrium adsorption method had still high crystallinity, while the intensities of the diffraction lines due to the MOF became weak with increase in the Pd loadings. Such decrease of the diffraction line intensities can be attributed to a certain loss of crystallinity or due to the presence of heavy metal (Pd) which scatters incident X-ray.[34] As shown in **Figure S1**, since there was no difference in the diffraction line intensities between before and after the reduction with $NaBH_4$, it is highly unlikely that X-ray scattering by Pd was the reason for the decrease of the diffraction line intensities. As will be mentioned later, since the surface area of NH_2-MIL-53 was decreased after the introduction of Pd NPs, partial decomposition of the framework structure of NH_2-MIL-53 during the introduction of Pd in the equilibrium adsorption method was more plausible. While the $PdCl_2$ solution was not concentrated in the equilibrium adsorption method unlike the case in the conventional impregnation method, the solution was weakly acidic (pH 4) and thus the framework structure of NH_2-MIL-53 might be partly decomposed in that solution. It should be noted that characteristic diffraction lines corresponding to Pd^0 particles were not observed for Pd@NH_2-MIL-53, suggesting that well-dispersed Pd NPs were formed even for the samples with high Pd loadings like 3.5 wt.% Pd.

The morphology of the pristine NH_2-MIL-53 and those after the introduction of Pd NPs with different preparation methods were investigated by SEM. As shown in **Figures 3a** and **3b**, the pristine NH_2-MIL-53 was composed of small spherical particles with particle size in the range of 10–20 nm. After the introduction of Pd by the conventional impregnation method (Pd/NH_2-MIL-53), morphological collapse, which was that the surface of the crystal agglomerates turned rougher and the agglomerates looked to be dissolved, was observed (**Figure 3c**). In contrast, such morphological change was not significant for Pd@NH_2-MIL-53 prepared by the equilibrium adsorption method (**Figure 3d**).

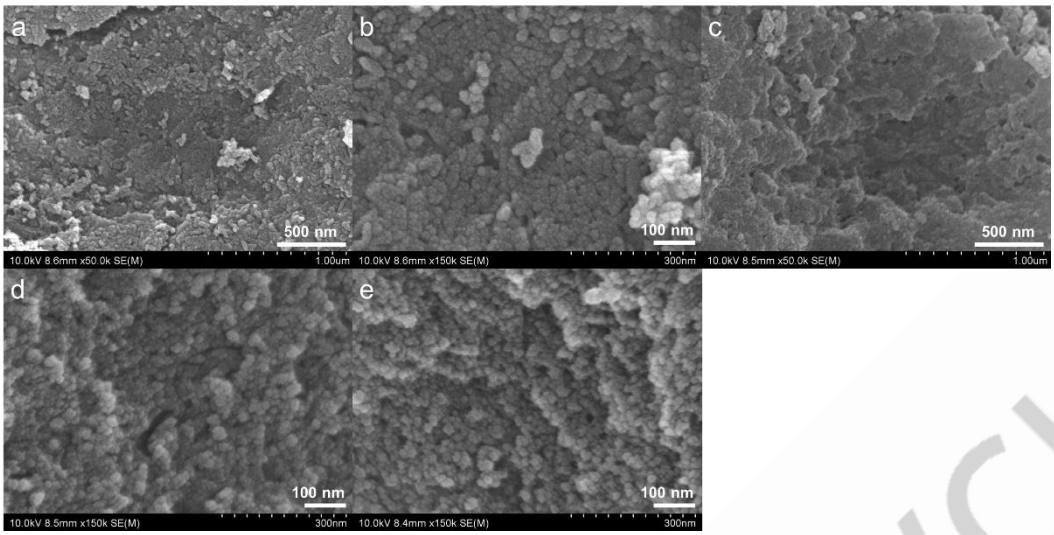

Figure 3. SEM images of (a, b)pristine NH_2-MIL-53 with low and high magnifications, respectively, (c)Pd/NH_2-MIL-53, (d)Pd@NH_2-MIL-53_0.8, and (e)Pd@NH_2-MIL-53_2.1.

Besides, no significant morphological change was observed even when the Pd loading was increased (**Figure 3e**).

N_2 adsorption isotherms for NH_2-MIL-53, Pd/NH_2-MIL-53 and Pd@NH_2-MIL-53 as well as pristine MIL-53 and Pd/MIL-53 are provided in **Figure 4**. The specific surface areas of the samples are also listed in **Table 1**. A sharp increase in the adsorption amount was observed at very low P/P_0 for pristine MIL-53 and NH_2-MIL-53, indicating the presence of well-developed micropores.[35-37] The specific surface areas of the pristine MIL-53 and NH_2-MIL-53 were 1042 and 401 $m^2\ g^{-1}$, respectively, where the former was in good agreement with the value in the published paper.[32] Despite of high crystallinity of NH_2-MIL-53 confirmed by PXRD (**Figure 3**), it had rather low specific surface area comparing with MIL-53. This might be due to the presence of carbon residue inside the pores, which was formed during the thermal treatment to remove DMF, blocking the micropores. The presence of such carbon residue was confirmed from the results of chemical elemental analysis (**Table S1**).

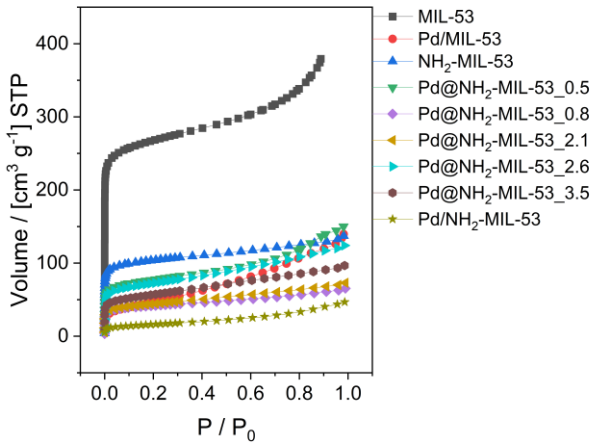

Figure 4. N_2 adsorption isotherms of MOFs and MOF-based catalysts.

After the Pd introduction by the conventional impregnation method, the surface areas were significantly decreased for both Pd/MIL-53 and Pd/NH_2-MIL-53 (**Table 1**), which was due to the collapse of the framework structure. In contrast, although the surface area was decreased due to partial collapse of the framework structure, the extent of the decrease was not so significant for Pd@NH_2-MIL-53. Based on these results, we concluded that the equilibrium adsorption method provided a good way capable to introduce Pd NPs to NH_2-MIL-53 with almost keeping the framework structure of the MOF.

Figure 5 shows TEM images of Pd@NH_2-MIL-53 with different Pd loadings. It was clearly observed that the Pd NPs were uniformly dispersed over Pd@NH_2-MIL-53, and bulky aggregate was not found even with high Pd loadings. The sizes of Pd NPs were distributed in the range of 0.6–4 nm with ca. 2 nm on average, regardless of the Pd loadings (**Table 2**). The presence of Pd NPs in Pd@NH_2-MIL-53 was also confirmed by EDX spectra of the samples (**Figure S2**). In contrast, Pd/MIL-53 and Pd/NH_2-MIL-53 prepared by the conventional impregnation method displayed larger particle size in the range of 0.8–14 nm

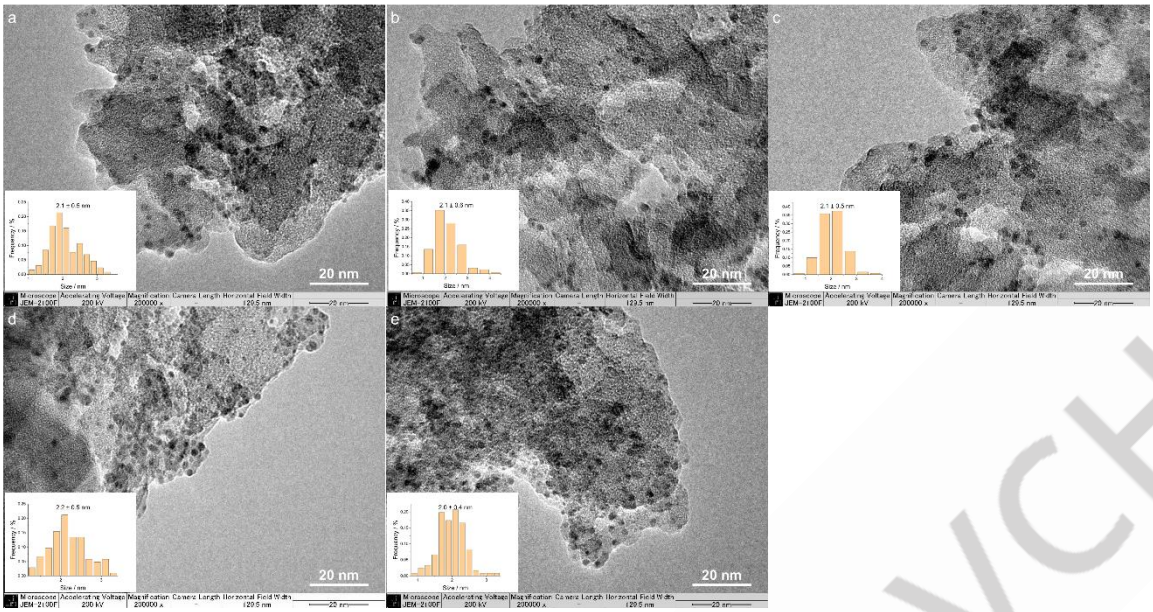

Figure 5. TEM images of (a) Pd@NH_2-MIL-53_0.5, (b)Pd@NH_2-MIL-53_0.8, (c)Pd@NH_2-MIL-53_2.1, (d)Pd@NH_2-MIL-53_2.6, and (e)Pd@NH_2-MIL-53_3.5.

(**Figure S3**), where some Pd particles were aggregated, forming large particles especially for Pd/MIL-53. These results demonstrated that applying NH_2-MIL-53 as a support material and using the equilibrium adsorption method were able to provide uniform Pd NPs even for high Pd loadings.

To investigate the difference in the structure of the surface of Pd NPs, IR spectra of CO adsorbed on the Pd-introduced MOFs were taken at 298 K. **Figure 6** shows the IR spectra of CO for Pd@NH_2-MIL-53 with different Pd loadings, where the spectra were taken after CO adsorption and subsequent N_2 purge at 298 K. Despite even after N_2 purge, two weak bands attributed to gas phase CO was still present at around 2170 and 2120 cm^{-1}. While the IR bands of CO for Pd@NH_2-MIL-53_0.5 were weak and the spectrum was little noisy because of small number of the Pd sites, a broad band dividable into two peaks at 2090 and 2070 cm^{-1}, and another broad one at around 1935 cm^{-1} were observed.

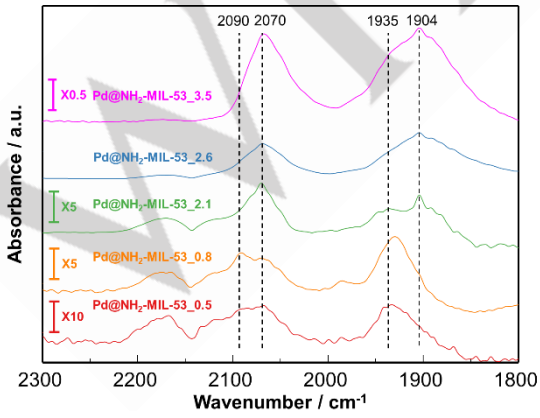

Figure 6. IR spectra of CO adsorbed on Pd@NH2-MIL-53 with different Pd loadings taken at 298 K.

In a previous paper by Szanyi and Kwak,[38] linear a-top CO adsorbed on Pd(111) and Pd(100) gave absorption bands at 2095~2099 and 2082 cm^{-1}, respectively, and the bands assignable to bridge-bounded CO on Pd(100) and Pd(111) were observed at 1970~1990 and 1939~1948 cm^{-1}, respectively. Similarly, Murata et al. assigned the band at approximately 2075 cm^{-1} to linear CO adsorbed on a corner site of Pd NPs and on Pd(111), and they also pointed out not to be able to distinguish between the two only from the band position.[39] In case of our Pd@NH_2-MIL-53_0.5, all absorption bands appeared at the positions similar to those reported by Szanyi and Kwak,[38] while slightly shifted towards low wavenumbers. Such shift was caused by the change in electronic state of Pd sites, which is presumably due to interaction between the amino group and Pd NPs in Pd@NH_2-MIL-53_0.5. Anyway, according to the assignment by Szanyi and Kwak,[38] we assigned the absorption bands of 2090, 2070 and ca. 1932 cm^{-1} for Pd@NH_2-MIL-53_0.5 to linear a-top CO on Pd(111) and Pd(100), and bridge-bound CO on Pd(111), respectively.

Pd@NH_2-MIL-53_0.5 and Pd@NH_2-MIL-53_0.8 showed similar IR spectra, indicating that the facets and electronic state of Pd NPs in the two catalysts were basically identical. With increase in the Pd loading to 2.1 wt.%, the absorption band at 2090 cm^{-1} became weak, being only a shoulder, and instead the band at 2070 cm^{-1} was dominant. In addition, intensity of the band at 1935 cm^{-1} was decreased, and that at 1904 cm^{-1}, which was assignable to the three-fold hollow-bound CO on Pd(111),[38-43] appeared. It should be noted that further increase in the Pd loadings, namely 2.6 and 3.5 wt.% Pd, such characteristics was more noticeable and the absorption band at 2090 cm^{-1} almost disappeared. The change in the IR spectra associated with the increase in the Pd loadings suggested that Pd(100) facet became dominant for the high Pd loading catalysts. The reason why exposure of Pd(100) facet was preferred in Pd@NH_2-MIL-53 with high Pd loadings may relate to kinetics for the formation of Pd NPs and thermodynamic stability of each facet. Since Pd atoms are more densely packed on Pd(111) than on Pd(100), the former facet is thermodynamically more stable. Thus, the thermodynamically stable Pd(111) facet was preferentially exposed for Pd@NH_2-MIL-53 with low Pd loadings, implying slow

particle growth. In contrast, Pd@NH_2-MIL-53 with high Pd loadings had a large amount of the Pd precursors, $(PdCl_3)^-$, and the reduction of the Pd precursors with $NaBH_4$ would generate many Pd^0 atoms at once, leading to the high concentration of Pd^0 atoms on NH_2-MIL-53. Such situation might facilitate the rapid formation of Pd NPs, resulting in thermodynamically less stable Pd NPs exposing Pd(100) facet, namely kinetically controlled formation of Pd NPs.

Generally, parameters such as reaction time, capping agents and precursor concentration must affect the nucleation and growth process in colloids formation.[44,45] It is known that halide ions acted as capping agents for Pd nanocrystals and the morphology of nanocrystals were changed depending on their presence or absence and concetration.[45,46] For example, bromine ion (Br^-) selectively adsorbed onto the (100) facet of Pd particle during its growth, and thus Pd nanocubes exposing (100) facet were formed in the presence of Br^-.[45,47,48] It is also demonstrated that the formation of Pd nanocubes was promoted in the presence of chloride ion,[49,50] where dominant Pd(100) facets were favoured with higher Cl^- concentration.[50] In this study, chloride ion (Cl^-) was generated in the solution upon the reduction of the Pd precursor and might act as capping agent in the Pd NPs growth. Since the ratio of Cl^- to Pd was almost constant, which was three, regardless of the Pd loadings as mentioned before, the capping effect of Cl^- on Pd NPs growth was probably almost identical regardless of the Pd loadings. Thus, it is likely that Pd NPs with almost the same size were formed in Pd@NH_2-MIL-53 with different Pd loadings, while the exposed facets were different.

We also measured IR spectra of CO adsorbed on Pd/NH_2-MIL-53 and Pd/MIL-53 (**Figure S4**). The IR spectrum of CO adsorbed on Pd/NH_2-MIL-53 was similar to that on Pd@NH_2-MIL-53_2.6 where two main bands corresponding to linear a-top CO on Pd(100) at 2070 cm^{-1} and three fold hollow-bound CO on Pd(111) at 1904 cm^{-1} were observed. Differently, Pd/MIL-53 exhibited absorption bands of linear a-top CO and bridge-bound CO on Pd(111) at 2077 and 1941 cm^{-1}, respectively, which located at a little higher wavenumbers compared to those for Pd@NH_2-MIL-53. Such difference in the band positions between Pd/MIL-53 and Pd@NH_2-MIL-53 also suggested the difference in the electronic state of Pd NPs,[51,52] and that the electronic state of Pd NPs in Pd@NH_2-MIL-53 was more negative than that in Pd/MIL-53, which might be caused by the interaction between amino group and Pd NPs in Pd@NH_2-MIL-53, promoting to the charge transfer from amino groups to Pd NPs.

Catalytic performances

The catalytic performances of Pd@MOFs were evaluated with the reduction of NO_2^- in water. **Figure 7** shows time dependence of NO_2^- conversion for Pd@NH_2-MIL-53 with different Pd loadings. While pristine NH_2-MIL-53 was inactive for the reaction, Pd@NH_2-MIL-53 effectively promote the reduction of NO_2^-. The catalytic activity was significantly changed depending on the Pd loadings and Pd@NH_2-MIL-53 with high Pd loadings were more active, which was firstly due to the large number of the surface Pd sites. In fact, almost 100 % NO_2^- conversion was achieved at 4 h for Pd@NH_2-MIL-53_2.1, Pd@NH_2-MIL-53_2.6, and Pd@NH_2-MIL-53_3.5. In contrast to the catalytic activity, all Pd@NH_2-MIL-53 exhibited similar selectivity and almost no NH_3 was formed whole the reaction time regardless of the Pd loadings. That is, we need to think about only the difference in the activity between the catalysts with different Pd loadings.

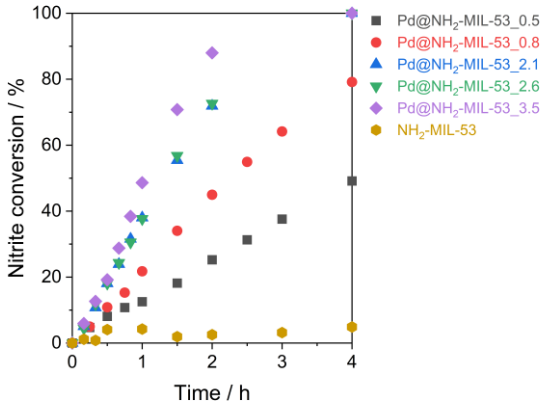

Figure 7. Time dependences of NO_2^- conversion for reduction of NO_2^- in water over Pd@NH_2-MIL-53 with different Pd loadings. Reaction conditions: catalyst weight, 20 mg; $[NO_2^-]_0$, 6.67 mmol L^{-1}; H_2 flow rate, 50 mL min^{-1}; and temperature, 298 K.

To quantitively evaluate the catalytic performances, the catalytic reaction data below 20% NO_2^- conversion were analysed using a pseudo-first-order reaction rate equation (**Figure S5**), giving rate constants (k_{obs}) and those are listed in **Table 2**. This table also includes specific activity per surface Pd sites (k_s) as well as average sizes and dispersions of Pd NPs. To estimate k_s, we assumed that the shape of Pd NPs was spheric,[53-55] and used the average size of Pd NPs (d) and the actual Pd loading obtained by TEM and ICP-AES, respectively. It is noted that k_s were changed depending on the Pd loadings, though the average sizes of Pd NPs were almost the same for all Pd@NH_2-MIL-53. The catalysts with low Pd loadings like Pd@NH_2-MIL-53_0.5 and Pd@NH_2-MIL-53_0.8 had large k_s, which were about 2.5 times as large as those for Pd@NH_2-MIL-53 with high Pd loadings. These results suggested that the structure and electronic state of the surface of Pd NPs also dominated the catalytic activity in addition to the number of the surface Pd sites. However, as demonstrated by Pd 3d XPS spectra (**Figure S6**), the electronic state of the surface of Pd NPs was basically identical regardless of the Pd loadings. Therefore, it is more plausible that the difference in the structure dominated the specific catalytic activity of Pd NPs on Pd@NH_2-MIL-53.

Table 2. Particle size and dispersion of Pd NPs in Pd@NH_2-MIL-53, and the catalytic performance for the reduction of NO_2^- in water.

Catalyst	d (nm)	D (%)	k_{obs} (h^{-1})	k_s (mol_{NO2^-} $mol_{surface\ Pd}^{-1}$ h^{-1})
Pd@NH_2-MIL-53_0.5	2.1	53	0.13	2.9×10^2
Pd@NH_2-MIL-53_0.8	2.1	53	0.24	3.0×10^2
Pd@NH_2-MIL-53_2.1	2.1	53	0.42	1.7×10^2
Pd@NH_2-MIL-53_2.6	2.2	51	0.41	1.3×10^2
Pd@NH_2-MIL-53_3.5	1.9	59	0.50	1.2×10^2
Pd/MIL-53	3.6	31	0.49	1.7×10^2
Pd/NH_2-MIL-53	3.6	31	0.33	1.8×10^2

To gain an insight into the reason why the difference in the Pd loadings made that in the specific catalytic activity per Pd sites (k_s), the absorption bands of CO adsorbed on Pd@NH_2-MIL-53 were deconvoluted using a Gaussian function and the absorption band areas of 1904, 1932, 2070, and 2090 cm^{-1} were calculated to estimate the fraction of each band area for Pd@NH_2-MIL-53 (**Table S2**) to investigate the correlation between those and k_s. After several trials, we found that k_s were correlated well with the fraction of the band areas of CO on Pd(111) facet (i.e. sum of the fractions of the band areas at 2090 and 1932 cm^{-1}) as shown in **Figure 8**. This correlation suggested that the highly active Pd sites were present on Pd(111) facet of Pd NPs. From the y-intercept and slope of the straight line in **Figure 8**, it was estimated that the specific activity of the active sites present on Pd(111) facet was about 6 times higher than that on the others, if absorption coefficients were the same each other. The reason for the high specific activity of Pd(111) facet is still not well understood, but low adsorption energy of a reaction intermediate may lead to the high specific activity. In previous studies, it was suggested that the adsorption of NO_2^- on Pd particles was energetically favoured and adsorbed NO_2^- was easily converted to NO, while formed NO was quite stable on the surface.[56-58] Moreover, it was suggested by DFT calculation that the rate constant for the reduction of NO_2^- was much larger than that of NO, and the adsorption of NO was much stronger than that of NO_2^- or H_2, suggesting that the adsorbed NO was stable and thus the reduction of NO was a rate-limiting step in the reduction of NO_2^-, leading to the accumulation of NO on the surface. While there was no significant difference in the adsorption energy for NO_2^- on different facets of Pd particles, the adsorption of NO was much stronger on Pd(100) facet than on other ones including Pd(111).[58] Thus, in our case, it is deduced that the strong adsorption of intermediate NO on Pd(100) facet hindered the further reduction of NO, while the weaker adsorption of NO on Pd(111) facet rendered the higher reaction activity exhibited on that facet.

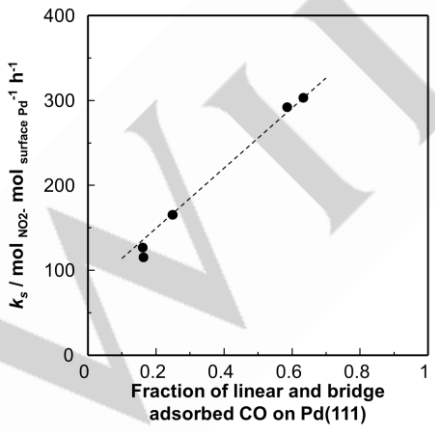

Figure 8. Plot of ks against the fraction of the band areas due to linear and bridge adsorbed CO on Pd(111).

Pd/NH_2-MIL-53 showed similar specific activity (k_s) to Pd@NH_2-MIL-53_2.1, but did lower than those of the low Pd loading Pd@NH_2-MIL-53 (0.5 and 0.8 wt.% Pd). This was resulted from the lower fraction of Pd(111) facet for Pd/NH_2-MIL-53. Despite of the higher fraction of Pd(111) facet for Pd/MIL-53 compared with Pd/NH_2-MIL-53, Pd/MIL-5 showed only similar specific activity (k_s) to Pd/NH_2-MIL-53. The reason for it might be that the electronic state of Pd NPs in Pd/NH_2-MIL-53 was more negative than that in Pd/MIL-53, as suggested by the band shift shown in the CO-IR spectrum. The higher electron density of Pd NPs in Pd/NH_2-MIL-53 promoted the NO_2^- reduction much more, and thus Pd/NH_2-MIL-53 had k_s similar to that for Pd/MIL-53, despite the fraction of Pd(111) facet in Pd/NH_2-MIL-53 was lower than that in Pd/MIL-53.

Conclusion

MIL-53 and NH_2-MIL-53 were applied as a support for introducing Pd particles and the catalytic performance of the resulting catalysts were evaluated with NO_2^- reduction in water. The amino group in NH_2-MIL-53 played a critical role in the introduction of the Pd precursor, which was $(PdCl_3)^-$, and Pd nanoparticles were successfully formed on NH_2-MIL-53 but it was failed for MIL-53 by the equilibrium adsorption method. The Pd precursor in the acidic $PdCl_2$ solution was electrostatically interacted with the protonated amino group in NH_2-MIL-53 to form an ion pair of -NH_3^+---$(PdCl_3)^-$, leading to the successful introduction of Pd nanoparticles to NH_2-MIL-53. The combination of using NH_2-MIL-53 and applying the equilibrium adsorption method was a good way to facilitate uniform dispersion of Pd nanoparticles even for high Pd loadings. Pd@NH_2-MIL-53 with different Pd loadings exhibited different Pd surface structures, where a linear relation between the specific activity per surface Pd site and the fraction of Pd(111) facet was observed. The Pd(111) facet on Pd@NH_2-MIL-53 exhibited high catalytic activity for NO_2^- reduction in water.

Experimental section

Synthesis of MOFs (NH_2-MIL-53 and MIL-53)

NH_2-MIL-53 was synthesized according to the method in a reference[32] with small modifications. The organic linker, NH_2-H_2BDC (4.14 mmol), was dissolved in 6 mL of aqueous NaOH solution (1.5 mol L^{-1}) and the solution was stirred for 30 min at room temperature, forming dark yellow solution (**Solution 1**). Another solution (**Solution 2**) was prepared by dissolving $Al(NO_3)_3 \cdot 9H_2O$ (4.14 mmol) in 4 mL of Milli-Q water. Then, **Solution 2** was added dropwise at room temperature into **Solution 1** under vigorous stirring. After being stirred at room temperature for 24 h, the resulting yellow solid was separated by centrifugation and washed with Milli-Q water and ethanol. The collected solid was then dried at 373 K overnight, subsequently immersed in 30 mL of DMF at 423 K for 5 h to exchange free NH_2-H_2BDC remaining in the pore with DMF. Then the powder was collected by filtration, washed with ethanol and acetone, and was dried at 373 K overnight. The solid after drying was heated at 523 K for 3 h to evaporate and remove DMF.

MIL-53 was synthesized with the similar manner to that for NH_2-MIL-53, but H_2BDC was used as an organic linker instead of NH_2-H_2BDC.

Introduction of Pd to MOFs

Equilibrium adsorption method. Pd particles were introduced to NH_2-MIL-53 by the equilibrium adsorption method as follows.

NH_2-MIL-53 was dispersed in an aqueous $PdCl_2$ solution (10 mmol L^{-1}), whose pH was adjusted to 4 by adding NaOH in advance. After overnight stirring, the mixture was filtrated and the solid on the filter was washed with Milli-Q water (50 mL × 3 times), followed by drying at 373 K overnight. After that, the obtained solid was treated in an aqueous $NaBH_4$ solution (0.1 mol L^{-1}) at 298 K for 30 min to reduce Pd species, forming Pd particles. Then, the solid was collected by filtration, washed with Milli-Q water (50 mL × 3 times) and dried at 373 K overnight.

Pd@NH_2-MIL-53 with different Pd loadings (denoted as Pd@NH_2-MIL-53_x, x represents the actual Pd loading, wt.%) were also prepared by changing the concentration of $PdCl_2$ in the solution, while the volume of the solution was constant.

Conventional impregnation method. Introduction of Pd to MOFs (NH_2-MIL-53 and MIL-53) were also conducted by a conventional impregnation method. MOF was dispersed in an aqueous $PdCl_2$ solution (10 mmol L^{-1}) and then, the suspension was evaporated at 323 K with a rotary evaporator to remove the solvent. The resulting solid was dried at 373 K overnight and treated with $NaBH_4$ as for Pd@NH_2-MIL-53. These catalysts prepared by the impregnation method are denoted as Pd/NH_2-MIL-53 and Pd/MIL-53.

Characterization

Powder X-ray diffraction (PXRD) patterns were collected on an X-ray diffractometer (D2 Phaser, Bruker) using Cu K_α radiation at a 0.02° step in the 2θ range of 5° to 50°. The surface area and pore volume were estimated from a N_2 adsorption isotherm taken at 77 K (BELSORP mini, BEL Japan, Inc). Before measurement, a sample was treated in N_2 flow at 403 K for 2 h. The specific surface area was calculated by applying Brunauer-Emmett-Teller (BET) equation to an adsorption isotherm in the P/P_0 range of 0.05 to 0.3. Morphology of the sample was observed by a field emission scanning electron microscopy (FE-SEM, S4800, HITACH). Particle size distribution and mean particle size of Pd particles in the samples were estimated from transmission electron microscope (TEM) images taken on a transmission electron microscope (JEM 2100F, JEOL) with electron acceleration voltage of 200 kV.

Fourier transform infrared (FT-IR) spectra of CO adsorbed on the samples were recorded on an IR spectrometer (FT/IR-6100, JASCO Co.) equipped with an MCT detector. About 40 mg of the sample was pressed into a self-supporting disk, and the sample disk was placed in a quartz IR cell equipped with CaF_2 windows connected to a gas flow system. The sample disk was heated in H_2 flow (10 mL min^{-1}) at 373 K for 30 min and then cooled to 298 K in N_2 flow (30 mL min^{-1}) in the cell. After the temperature reached to 298 K, 5% CO in N_2 was contacted with the sample disk for 10 min. After that, the gas was switched to N_2 to remove weakly adsorbed CO and IR spectrum was recorded at 298 K.

The content of Pd in the samples was quantified using an inductively coupled plasma-atomic emission spectrometer (ICPE-9000, Shimazu Co.). The samples were calcined at 1073 K for 3 h to combust all the organic moieties and the resulting solid was treated with an aqueous $NaBH_4$ solution to reduce oxidized Pd species to Pd^0. Then, all the solid was dissolved in aqua regia and the solution was diluted with Milli-Q water to afford the measurement.

Chemical elemental analyses of C, H and N for the samples were carried out with a CHN analyser (CE440, Exeter Analytical, Inc) at Global Facility Center, Hokkaido University. For Cl^- analysis, the sample was dissolved in a concentrated aqueous NaOH solution, and the solution was analysed by ion chromatography (IC) in the same way as the analysis for NO_2^- in reaction solution.

Evaluation of catalytic performance

Reduction of NO_2^- with H_2 in water was carried out in a round-bottom flask connected with a gas flow system. Normally, catalyst (ca. 20 mg), 100 mL of aqueous $NaNO_2$ solution (10 mmol L^{-1}) and 50 mL of Milli-Q water were put in the flask, where the concentration of NO_2^- was 6.67 mmol L^{-1}. After bubbling N_2 (30 mL min^{-1}) into the reaction solution for 30 min to remove dissolved air, mixed gas composed of H_2 (50 mL min^{-1}) and CO_2 (50 mL min^{-1}) was flown to start the reaction. The reaction was conducted at room temperature (298 K) for 4 h with magnetic stirring (500 rpm). To trap formed NH_3, two traps with diluted H_2SO_4 were connected at the outlet of the reactor.

A small portion of the reaction solution (1 mL) was taken at regular time interval and centrifuged to separate catalyst from the solution. The concentration of NO_2^- in supernatant was measured using an ion chromatograph (IC-8100, Tosoh) equipped with a TSK gel Super IC-AZ column. The concentration of ammonium ion (NH_4^+) in the reaction and trap solutions was determined using another ion chromatograph (IC-2001 Tosoh,) equipped with a TSK gel Super IC-CR column.

Reaction rate constant was calculated from the data at conversion of NO_2^- less than 20%, assuming pseudo-first-order reaction for NO_2^- concentration (**equation 1**),

$$-\frac{d[NO_2^-]}{dt} = k_{obs} \times [NO_2^-] \quad (1)$$

where $[NO_2^-]$ and k_{obs} are concentration of NO_2^- at reaction time t and pseudo-first-order rate constant, respectively.

Specific activity per surface Pd site (k_s, mmol h^{-1} $mmol_{Pd}^{-1}$), which is so-called turnover frequency, for NO_2^- reduction was calculated by dividing the pseudo-first-order rate constant (k_{obs}) and the initial NO_2^- amount ($n_{nitrite}$, mmol) by the number of the Pd sites exposed on the surface ($n_{surface\ Pd}$, mmol) as **equation 2**,

$$k_s = \frac{k_{obs} \times n_{nitrite}}{n_{surface\ Pd}} = \frac{k_{obs} \times n_{nitrite}}{n_{Pd} \times D} \quad (2)$$

where D is dispersion of Pd (i.e., fraction of the number of Pd exposed on the surface to the total number of Pd in the catalyst) and was calculated from the average Pd particle size estimated from TEM images, assuming that the shape of Pd particles was spherical,[53-55] n_{Pd} is the total Pd amount (mol) in the catalyst.

Selectivity to NH_4^+ ($S_{NH_4^+}$) was calculated according to **equation 3**.

$$S_{NH_4^+} = \frac{[NH_4^+]_t}{[NO_2^-]_0 - [NO_2^-]_t} \times 100 \quad (3)$$

Selectivity to N_2 was calculated by assuming that only N_2 and NH_4^+ were the end-products in the reaction (**equation 4**).

$$S_{N_2} = 100 - S_{NH_4^+} \quad (4)$$

Supporting Information

The authors have cited additional references within the Supporting Information.

Acknowledgements

The authors thank the Open Facility, Global Facility Center, Creative Research Institute, Hokkaido University for allowing the authors to conduct the analysis with ICP-AES, TEM and elemental analysis. This work was supported by JSPS KAKENHI Grant Number 21H01709 and JST SPRING, Grant Number JPMJSP2119. A part of this work was supported by "Advanced Research Infrastructure for Materials and Nanotechnology in Japan (ARIM)" of the Ministry of Education, Culture, Sports, Science and Technology (MEXT). Grant Number JPMXP1224HK0049 (Hokkaido University).

We also thank Dr. Ryota Osuga (Institute for Catalysis, Hokkaido University) for helping us to perform STEM-EDX analyses.

Keywords: Metal-organic framework · Palladium · Nitrite reduction · Water · High metal loading

References

1. H. C. Zhou, J. R. Long and O. M. Yaghi, *Chem. Rev.* **2012**, *112*, 673-674.
2. H. C. Zhou and S. Kitagawa, *Chem. Soc. Rev.* **2014**, *43*, 5415-5418.
3. M. Fujita, Y. J. Kwon, S. Washizu and K. Ogura, *J. Am. Chem. Soc.* **1994**, *116*, 1151-1152.
4. S. Hasegawa, S. Horike, R. Matsuda, S. Furukawa, K. Mochizuki, Y. Kinoshita and S. Kitagawa, *J. Am. Chem. Soc.* **2007**, *129*, 2607-2614.
5. A. Dhakshinamoorthy, M. Alvaro, H. Garcia, *Chem. Commun.* **2012**, *48*, 11275-11288.
6. Z. G. Hu, D. Zhao, *CrystEngComm* **2017**, *19*, 4066-4081.
7. L. L. Liu, Y. B. Song, H. B. Chong, S. Yang, J. Xiang, S. Jin, X. Kang, J. Zhang, H. Z. Yu, M. Z. Zhu, *Nanoscale* **2016**, *8*, 1407-1412.
8. B. An, J. Z. Zhang, K. Cheng, P. F. Ji, C. Wang, W. B. Lin, *J. Am. Chem. Soc.* **2017**, *139*, 3834-3840.
9. S. F. Ji, Y. J. Chen, S. Zhao, W. X. Chen, L. J. Shi, Y. Wang, J. C. Dong, Z. Li, F. W. Li, C. Chen, Q. Peng, J. Li, D. S. Wang, Y. D. Li, *Angew. Chem. Int. Ed.* **2019**, *58*, 4271-4275.
10. K. L. Kollmannsberger, L. Kronthaler, J. R. Jinschek, R. A. Fischer, *Chem. Soc. Rev.* **2022**, *51*, 9933-9959.
11. X. C. Ma, C. Pu, Y. X. Zhang, G. G. Chang, G. Tian, S. M. Wu, J. W. Liu, Z. Y. Hu, L. Y. Wang, Y. X. Yin, C. Janiak, X. Y. Yang, *Chem. Eng. J.* **2022**, *429*, 132128.
12. X. L. Li, T. W. Goh, L. Li, C. X. Xiao, Z. Y. Guo, X. C. Zeng, W. Y. Huang, *ACS Catal.* **2016**, *6*, 3461-3468.
13. Y. Z. Chen, Z. U. Wang, H. W. Wang, J. L. Lu, S. H. Yu, H. L. Jiang, *J. Am. Chem. Soc.* **2017**, *139*, 2035-2044.
14. M. Meilikhov, K. Yusenko, D. Esken, S. Turner, G. Van Tendeloo, R. A. Fischer, *Euro. J. Inorg. Chem.* **2010**, 3701-3714.
15. H. R. Moon, D. W. Lim, M. P. Suh, *Chem. Soc. Rev.* **2013**, *42*, 1807-1824.
16. Q. H. Yang, Q. Xu, H. L. Jiang, *Chem. Soc. Rev.* **2017**, *46*, 4774-4808.
17. Q. Wang, D. Astruc, *Chem. Rev.* **2020**, *120*, 1438-1511.
18. K. M. Choi, K. Na, G. A. Somorjai, O. M. Yaghi, *J. Am. Chem. Soc.* **2015**, *137*, 7810-7816.
19. A. Dhakshinamoorthy, A. M. Asiri, H. Garcia, *Chem. Commun.* **2014**, *50*, 12800-12814.
20. C. H. Wang, X. L. Liu, N. K. Demir, J. P. Chen, K. Li, *Chem. Soc. Rev.* **2016**, *45*, 5107-5134.
21. T. Loiseau, C. Serre, C. Huguenard, G. Fink, F. Taulelle, M. Henry, T. Bataille, G. Férey, *Chem. Euro. J.* **2004**, *10*, 1373-1382.
22. U. Prüsse, M. Hähnlein, J. Daum, K. D. Vorlop, *Catal. Today* **2000**, *55*, 79-90.
23. R. Zhang, D. M. Shuai, K. A. Guy, J. R. Shapley, T. J. Strathmann, C. J. Werth, *ChemCatChem* **2013**, *5*, 313-321.
24. J. Hirayama, Y. Kamiya, *Catal. Sci. Technol.* **2018**, *8*, 4985-4993.
25. F. Deganello, L. F. Liotta, A. Macaluso, A. M. Venezia, G. Deganello, *Appl. Catal. B* **2000**, *24*, 265-273.
26. M. J. Chollier-Brym, R. Gavagnin, G. Strukul, M. Marella, M. Tomaselli, P. Ruiz, *Catal. Today* **2002**, *75*, 49-55.
27. Y. Yoshinaga, T. Akita, I. Mikami, T. Okuhara, *J. Catal*. **2002**, *207*, 37-45.
28. A. Pintar, J. Batista, I. Musevic, *Appl. Catal. B* **2004**, *52*, 49-60.
29. F. A. Marchesini, L. B. Gutierrez, C. A. Querini, E. E. Miró, *Chem. Eng. J.* **2010**, *159*, 203-211.
30. J. Martínez, A. Ortiz, I. Ortiz, *Appl. Catal. B* **2017**, *207*, 42-59.
31. M. Ruiz, A. M. Sastre and E. Guibal, *React. Funct. Polym.* **2000**, *45*, 155-173.
32. M. Sánchez-Sánchez, N. Getachew, K. Díaz, M. Díaz-García, Y. Chebude, I. Díaz, *Green Chem.* **2015**, *17*, 1500-1509.
33. I. J. Kang, N. A. Khan, E. Haque, S. H. Jhung, *Chem. Euro. J.* **2011**, *17*, 6437-6442.
34. R. Mahugo, A. Mayoral, M. Sánchez-Sánchez, I. Diaz, *Front. Chem.*, **2019**, 686.
35. L. Alaerts, M. Maes, L. Giebeler, P. A. Jacobs, J. A. Martens, J. F. M. Denayer, C. E. A. Kirschhock, D. E. De Vos, *J. Am. Chem. Soc.* **2008**, *130*, 14170-14178.
36. X. Q. Cheng, A. F. Zhang, K. K. Hou, M. Liu, Y. X. Wang, C. S. Song, G. L. Zhang, X. W. Guo, *Dalton Trans.* **2013**, *42*, 13698-13705.
37. H. N. Wamba, N. Singh, S. Dalakoti, S. Divekar, A. Arya, A. T. C. Kuate, J. Ngoune, S. Dasgupta, *ChemistrySelect*, **2023**, *8*, e202204476.
38. J. Szanyi, J. H. Kwak, *Phys. Chem. Chem. Phys.* **2014**, *16*, 15126-15138.
39. K. Murata, E. Eleeda, J. Ohyama, Y. Yamamoto, S. Arai, A. Satsuma, *Phys. Chem. Chem. Phys.* **2019**, *21*, 18128-18137.
40. E. Ozensoy, D. C. Meier, D. W. Goodman, *J. Phys. Chem. B* **2002**, *106*, 9367-9371.
41. G. Rupprechter, H. Unterhalt, M. Morkel, P. Galletto, L. J. Hu, H. J. Freund, *Surf. Sci.* **2002**, *502*, 109-122.
42. D. Tessier, A. Rakai, F. Bozonverduraz, *J. Chem. Soc., Faraday Trans.* **1992**, *88*, 741-749.
43. M. Skotak, Z. Karpinski, W. Juszczyk, J. Pielaszek, L. Kepinski, D. V. Kazachkin, V. I. Kovalchuk, J. L. d'Itri, *J. Catal.* **2004**, *227*, 11-25.
44. A. R. Tao, S. Habas, P. D. Yang, *Small* **2008**, *4*, 310-325.
45. H. Zhang, M. S. Jin, Y. J. Xiong, B. Lim and Y. N. Xia, *Acc. Chem. Res.* **2013**, *46*, 1783-1794.
46. Y. J. Xiong, J. Y. Chen, B. Wiley, Y. N. Xia, S. Aloni, Y. D. Yin, *J. Am. Chem. Soc.* **2005**, *127*, 7332-7333.
47. Y. J. Xiong, H. G. Cai, B. J. Wiley, J. G. Wang, M. J. Kim, Y. N. Xia, *J. Am. Chem. Soc.* **2007**, *129*, 3665-3675.
48. B. Lim, H. Kobayashi, P. H. C. Camargo, L. F. Allard, J. Y. Liu, Y. N. Xia, *Nano Res.* **2010**, *3*, 180-188.
49. N. Nalajala, A. Chakraborty, B. Bera, M. Neergat, *Nanotechnology*, **2016**, *27*, 065603.
50. K. J. Sun, X. B. Sun, X. X. Zou, W. Y. Pang, X. F. Hao, Y. H. Xu, H. Y. Su, *Appl. Surf. Sci.* **2023**, *638*, 159175.

51. Z. Q. Zhang, W. X. Shi, W. Wang, Y. P. Xu, X. Bao, R. J. Zhang, B. Zhang, Y. Guo, F. Y. Cui, *Environ. Sci. Nano* **2018**, *5*, 338-349.
52. Y. Zhao, J. A. Baeza, N. K. Rao, L. Calvo, M. A. Gilarranz, Y. D. Li, L. Lefferts, *J. Catal.* **2014**, *318*, 162-169.
53. T. Lear, R. Marshall, J. A. Lopez-Sanchez, S. D. Jackson, T. M. Klapötke, M. Bäumer, G. Rupprechter, H. J. Freund, D. Lennon, *J. Chem. Phys.* **2005**, *123*, 174706.
54. J. J. Li, W. Chen, H. Zhao, X. S. Zheng, L. H. Wu, H. B. Pan, J. F. Zhu, Y. X. Chen, J. L. Lu, *J. Catal.* **2017**, *352*, 371-381.
55. Z. Q. Zhang, J. S. Lu, B. Zhang, W. X. Shi, Y. Guo, F. Y. Cui, *Environ. Sci. Nano*, **2020**, *7*, 2117-2129.
56. S. D. Ebbesen, B. L. Mojet, L. Lefferts, *J. Catal*. **2008**, *256*, 15-23.
57. H. Shin, S. Jung, S. Bae, W. Lee, H. Kim, *Environ. Sci. Technol.* **2014**, *48*, 12768-12774.
58. D. M. Shuai, D. C. McCalman, J. K. Choe, J. R. Shapley, W. F. Schneider, C. J. Werth, *ACS Catal.* **2013**, *3*, 453-463.

Entry for the Table of Contents

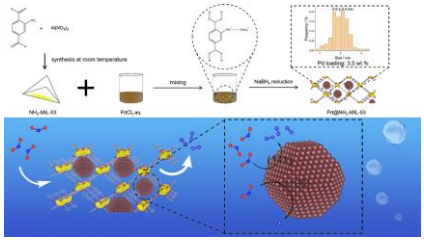

Pd nanoparticles (about 2 nm) with uniform distribution were formed on NH_2-MIL-53 despite of high loading, by a facile equilibrium adsorption method. The obtained catalysts showed high activity for catalytic reduction of nitrite in water, due to the preferential exposure of Pd(111) facets on Pd nanoparticles.

Supporting information

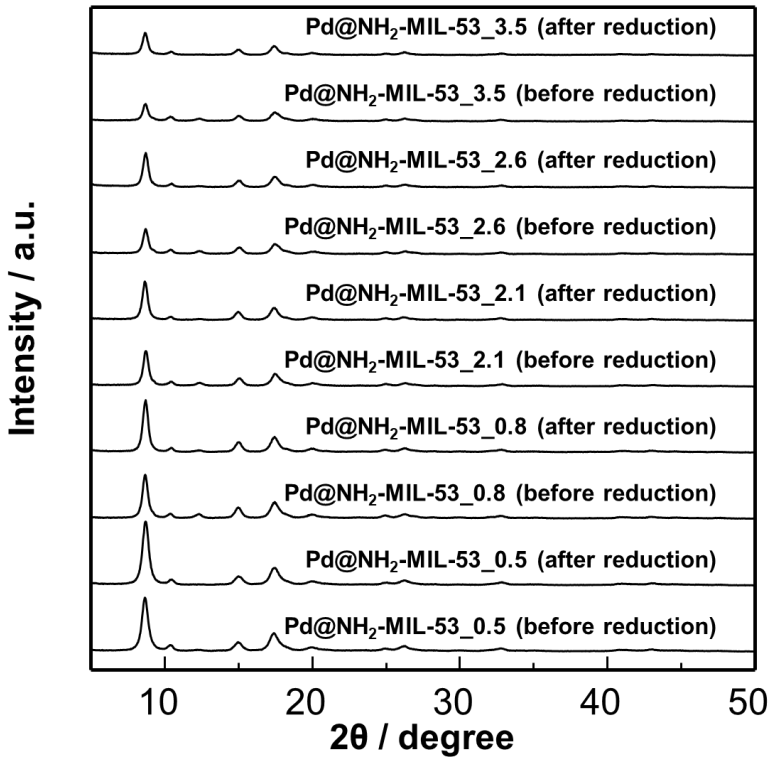

Figure S1. PXRD patterns of Pd@NH_2-MIL-53 before and after reduction with $NaBH_4$.

Table S1. Compositions of NH_2-MIL-53 at each step of the synthesis determined by elemental analysis.

Sample	Observed value (wt.%)			Atomic ratio
	C	H	N	N/C
As-synthesized NH_2-MIL-53	41.7	2.82	6.41	0.132
NH_2-MIL-53(after DMF exchange)	39.5	3.24	7.07	0.154
NH_2-MIL-53(after DMF and heat treatment)	32.2	2.58	4.45	0.118

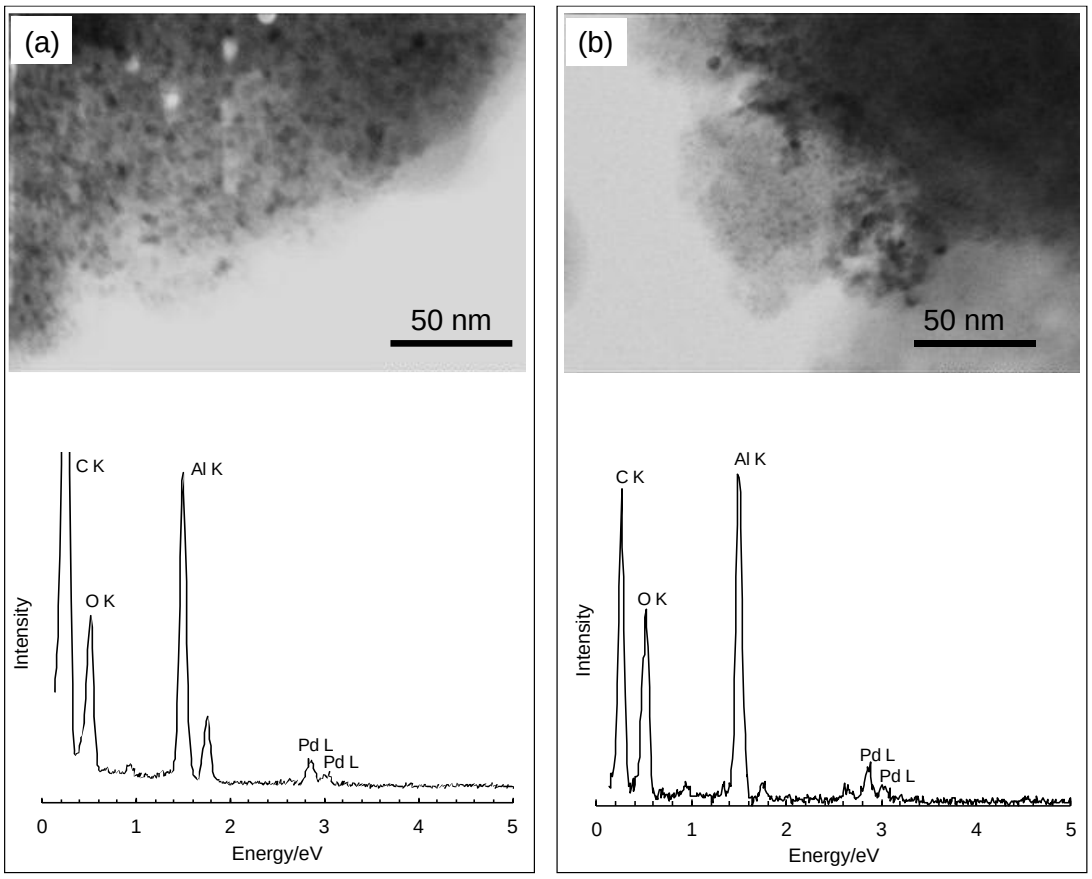

Figure S2. STEM images and EDX spectra of (a)Pd@NH_2-MIL-53_0.5 and (b)Pd@NH_2-MIL-53_3.5, which are the typical samples with low and high Pd loadings, respectively.

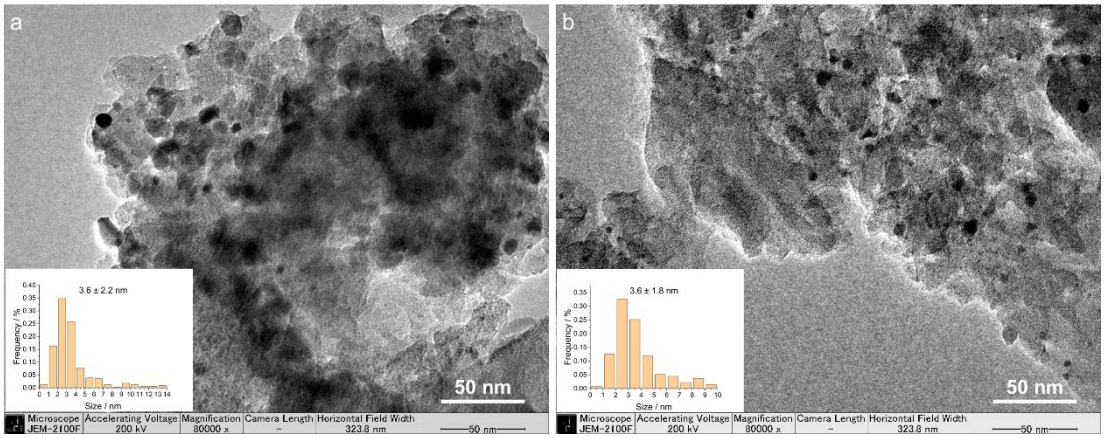

Figure S3. TEM images and particle size distributions of Pd NPs for (a)Pd/MIL-53 and (b)Pd/NH_2-MIL-53, which were prepared by a conventional impregnation method.

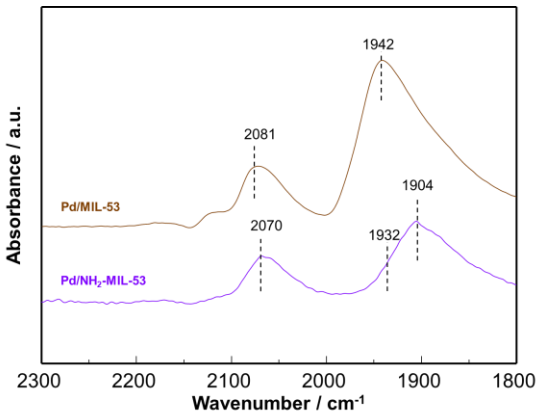

Figure S4. IR spectra of CO adsorbed on Pd/NH_2-MIL-53 and Pd/MIL-53 taken at 298 K.

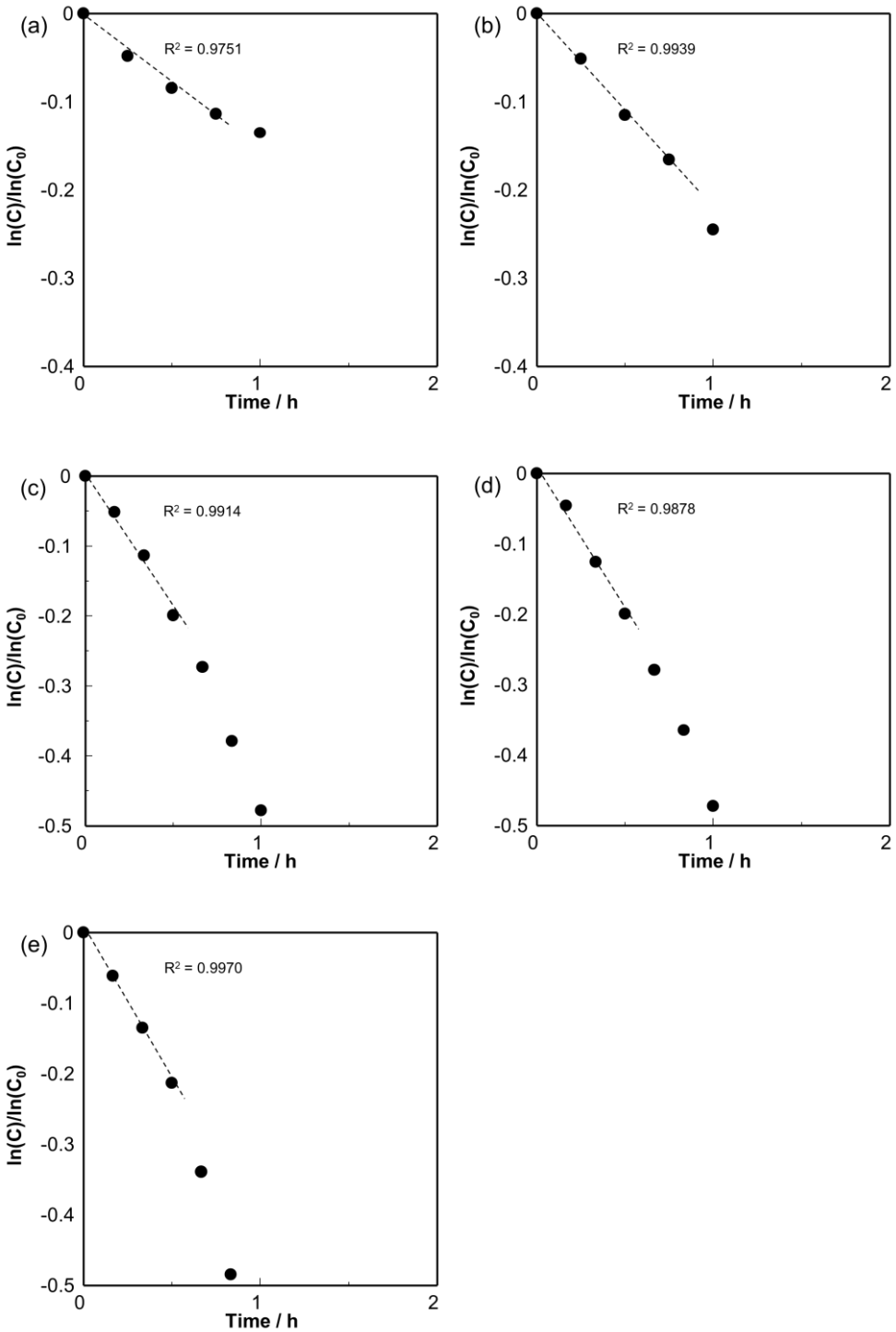

Figure S5. Plots of first-order reaction for nitrite reduction.

(a)Pd@NH_2-MIL-53_0.5, (b)Pd@NH_2-MIL-53_0.8, (c)Pd@NH_2-MIL-53_2.1, (d)Pd@NH_2-MIL-53_2.6 and (e)Pd@NH_2-MIL-53_3.5.

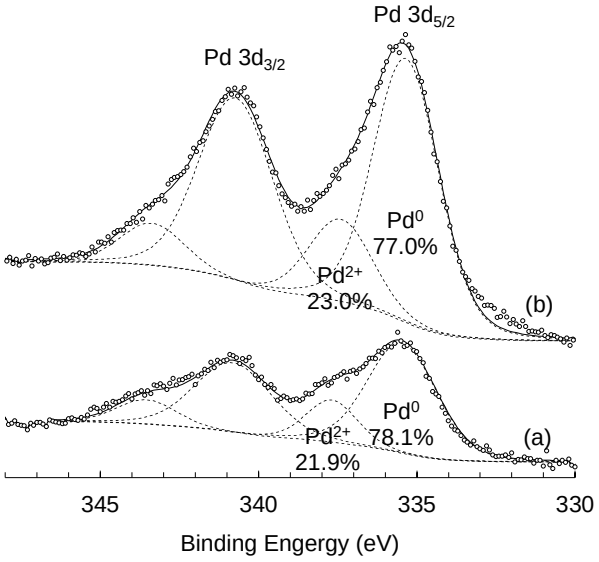

Figure S6. Pd 3d XPS spectra of (a)Pd@NH_2-MIL-53_0.5 and (b)Pd@NH_2-MIL-53_3.5.

Table S2. The fractions of the IR band area of different adsorbed CO species on Pd catalysts.

Catalyst	Linear a-top CO on Pd(111) (ca. 2090 cm^{-1})	Linear a-top CO on Pd(100) (ca. 2070 cm^{-1})	Bridge bound CO on Pd(111) (ca. 1932 cm^{-1})	Hollow CO on Pd(111) (ca. 1904 cm^{-1})
Pd@NH_2-MIL-53_0.5	0.18	0.29	0.41	0.06
Pd@NH_2-MIL-53_0.8	0.13	0.25	0.50	0.00
Pd@NH_2-MIL-53_2.1	0.14	0.22	0.11	0.40
Pd@NH_2-MIL-53_2.6	0.00	0.37	0.16	0.47
Pd@NH_2-MIL-53_3.5	0.00	0.32	0.16	0.46
Pd/MIL-53	0.00	0.24	0.11	0.57
Pd/NH_2-MIL-53	0.00	0.13	0.49	0.32